Journal of Applied Polymer Science

Metallopolymers based on a polyazomethine ligand containing rigid oxadiazole and flexible tetramethyldisiloxane units

Mirela-Fernanda Zaltariov, Maria Cazacu, Carmen Racles, Valentina Musteata, Angelica Vlad, Anton Airinei

Petru Poni Institute of Macromolecular Chemistry, Aleea Grigore Ghica Voda, 41A 700487, Iasi Romania

Correspondence to: M. Cazacu (E-mail: mcazacu@icmpp.ro)

ABSTRACT: Soluble, easily processable polymer–metal complexes with improved optical and dielectric properties for optoelectronic functional materials were obtained. For this, a new polyazomethine (PAZ2) was prepared by the reaction of a siloxane dialdehyde and bis(formyl-*p*-phenoxymethyl) tetramethyldisiloxane with 2,5-bis(*p*-aminophenyl)-1,3,4-oxadiazole, and it was used as a ligand for Cu(II), Co(II), and Zn(II) ions on the basis of the presence of the electron-donor nitrogen atoms from the azomethine group and oxadiazole ring. The structure of the PAZ2 was determined by spectral [Fourier transform infrared (FTIR) and ^{1}H-NMR spectroscopy] techniques. The metal complexation was proven by FTIR spectroscopy, and the silicon-to-metal ratios in the complexes were established by energy-dispersive X-ray fluorescence. The new materials were characterized by gel permeation chromatography, thermogravimetric analysis, and differential scanning calorimetry. The optical properties of PAZ2 and the derived metal complexes were studied by ultraviolet–visible and fluorescence spectroscopies. PAZ2 shows fluorescence emission, and it was significantly enhanced by metal complexation. The emission was enhanced by protonation; this behavior is useful, especially for sensors. The electrical properties were investigated by dielectric spectroscopy at various frequencies and temperatures, and this emphasized the existence of dipolar relaxations. © 2014 Wiley Periodicals, Inc. J. Appl. Polym. Sci. **2015**, *132*, 41631.

KEYWORDS: dielectric properties; optical properties; polycondensation; properties and characterization; thermal properties

Received 6 May 2014; accepted 12 October 2014

DOI: 10.1002/app.41631

INTRODUCTION

Polymeric metal complexes consist of metal centers in well-defined macromolecular environments. This is a growing field in the quest for synthetic materials with new properties derived from those of the individual organic and metal components. Thus, such polymers may be easily processable and have useful redox, catalytic, electrical, magnetic, and optical properties or may serve as precursors to novel ceramics.[1–3] There are several synthetic routes to these materials. In general, the methods include the complexation between a ligand group anchored on a polymer matrix and a metal ion,[4] the reaction of a multifunctional ligand with a metal ion, and the polymerization of metal-containing monomers.[5–12]

Among the different kinds of polymers, polyazomethines, also known as polyimines or Schiff-base polymers, have become an interesting class of polymers; they are useful as macromolecular ligands that coordinate to metal ions via an azomethine nitrogen.[13] The interest in this type of materials is due to their good properties: thermal, conducting, biological activity, fiber-forming, liquid-crystalline, and nonlinear optical properties,[14,15] which are useful for various application fields.[13] Polyazomethines (PAZs) also have the advantage of easy preparation in mild reaction conditions. The only byproduct is water, and the purification of the reaction product is relatively simple.[16]

PAZs are prepared by the polycondensation of diamino and dicarbonyl compounds to give high-molecular-weight polymers.[15] In general, these derivatives are aromatic components; the PAZs thus become an attractive class of high-performance polymers.[17,18] However, the rigidity of the PAZs and derived metal complexes causes high melting points and poor solubility in organic solvents; this limits their practical applications in various fields. To lower the transition temperatures and to improve their solubility, several methods have been used; these include the introduction of alkyl or alkoxy groups in the ortho position of the aromatic ring or the inclusion of flexible aliphatic spacers between the main-chain aromatic rings.[14,15,19,20] Various modified PAZs, such as poly(azomethine ester)s, poly(azomethine–ether)s, poly(azomethine–carbonate)s, poly(amide–azomethine-ester)s,

Additional Supporting Information may be found in the online version of this article.

poly(acrylate–azomethine)s, thermosetting PAZs, poly(azomethine-sulfone)s, and poly(azomethine–ether–sulfone)s, were also synthesized to reduce the melting temperature, improve the solubility, and promote specific properties, such as mesomorphism.[17,18] The inclusion of PAZ2s in rotaxane architecture is another strategy used to improve their processability.[21] Siloxane moieties have also been used as flexible spacers; often, poly(siloxane–azomethine)s exhibit liquid-crystalline behavior.[22–30]

Some time ago, we began to prepare different PAZs and derived metal complexes with at least a siloxane-based component (either carbonyl or amine).[4,10,11,25,26,31–33] We recently reported[33] the synthesis of new dialdehyde-containing dimethyl silane units, bis(formyl-*p*-phenoxymethyl) dimethyl silane, and its use in the preparation of PAZs. Here, we report the condensation of another new dialdehyde-containing, highly flexible tetramethyldisiloxane fragment, bis(formyl-*p*-phenoxymethyl) tetramethyldisiloxane,[32] with 2,5-bis(*p*-aminophenyl)-1,3,4-oxadiazole, as a photoactive component.[34–36] The resulting polyazomethine (PAZ2) was used as a ligand to coordinate Co, Cu, and Zn ions. The thermal, optical, and dielectric properties were investigated both for the ligand and the derived metal complexes.

EXPERIMENTAL

Materials

Bis(formyl-*p*-phenoxymethyl) tetramethyldisiloxane[32] and 2,5-bis(*p*-aminophenyl)-1,3,4-oxadiazole[33,34,37–40] were prepared and characterized according to published procedures.

Copper chloride dihydrate ($CuCl_2{\cdot}2H_2O$, purity $\geq$ 98%), cobalt chloride hexahydrate ($CoCl_2{\cdot}6H_2O$, purity $\geq$ 98%), and zinc chloride ($ZnCl_2$, anhydrous, purity = 99.99%) were purchased from Sigma-Aldrich.

The solvents methanol, ethanol, dimethyl sulfoxide (DMSO), dimethylformamide (DMF), petroleum ether, and chloroform (Chemical Co.) were used as received.

Methods

Fourier transform infrared (FTIR) spectra were recorded with a Bruker Vertex 70 FTIR spectrometer in transmission mode in the range 400–4000 cm^{-1} at room temperature with a resolution of 2 cm^{-1} and an accumulation of 32 scans.

Far-IR (FIR) spectra were recorded with a Bruker Vertex 70 FTIR spectrometer equipped with a FIR source, a CsI beam splitter, and a standard DLaTGS (standard deuterated L-alanine doped triglycine sulfate) detector. The spectra were obtained in transmission mode in the range 180–700 cm^{-1} at room temperature with a resolution of 2 cm^{-1} and an accumulation of 64 scans.

The ^{1}H-NMR spectra were acquired in hexadeuterated dimethyl sulfoxide (DMSO-d_6) at 25°C with a Bruker Avance DRX 400 MHz spectrometer operating at 400.13 MHz for ^{1}H. The spectrometer was equipped with a 5-mm four nuclei and a direct-detection *z*-gradient probe head. The chemical shifts are reported in parts per million (ppm) and are referenced to DMSO δ ^{1}H = 2.51 ppm.

Gel permeation chromatography (GPC) measurements were done with a PL-EMD 950 evaporative mass detector instrument. Calibration was done with polystyrene with molecular weights of 3,150,000 to 580 Da as standards, and DMF (1% solution) was used as the solvent (elution rate = 1 mL/min.)

The presence and ratio of metal and Si were evidenced with an energy-dispersive X-ray fluorescence (XRF) system (EX-2600 X-Calibur SDD).

Thermogravimetric (TG) measurements were conducted on an STA 449 F1 Jupiter device (Netzsch, Germany). About 10 mg of each sample was weighed and heated in alumina crucibles. Nitrogen was purged as an inert atmosphere at a flow rate of 50 mL/min. The samples were heated in the temperature range 30–900°C at a rate of 10°C/min. Differential scanning calorimetry (DSC) measurements were performed on a DSC 200 F3 Maia device (Netzsch, Germany). An amount of 10 mg of each sample was heated in pressed and pierced aluminum crucibles at a heating rate of 10°C/min. The cooling rate was also 10°C/min. Nitrogen was used as an inert atmosphere at a flow rate of 50 mL/min. The temperature against heat flow was recorded. We obtained the baseline by scanning the temperature domain of the experiments with an empty pan. The temperature and sensitivity calibrations were performed with five different metals at various heating rates according to standard procedures.

The electronic absorption spectra were measured with an Analytik Jena SPECORD 200 spectrophotometer in a 10-mm optical path quartz cells fitted with polytetrafluoroethylene stoppers. Fluorescence spectra were obtained with a PerkinElmer LS55 luminescence spectrometer in solution or in the solid state.

The dielectric measurements were performed with a Novocontrol broadband dielectric spectrometer Concept 40. The samples compressed at 10 t/cm^2 at room temperature to form pellets with a diameter of 13 mm and a thickness of 0.5 mm were placed between gold-plated round electrodes. We recorded the data isothermally by sweeping the frequency from 10 to 10^6 Hz at every 5°C interval in the range from −120 to 50°C. The temperature was controlled with a 0.1°C stability by a Novocontrol Quatro Cryosystem in a dry nitrogen atmosphere.

Procedure

Synthesis of PAZ2. In a 50-mL round-bottom flask fitted with a magnetic stirrer, reflux condenser, and $CaCl_2$ tube, a 2,5-bis(*p*-aminophenyl)-1,3,4-oxadiazole (0.252 g, 1 mmol) solution in DMF (5 mL) was introduced. To this solution, bis(formyl-*p*-phenoxymethyl) tetramethyldisiloxane (0.404 g, 1 mmol) dissolved in $CHCl_3$ (5 mL) was added, and the mixture was heated to reflux for 8 h; then, it was poured in 30 mL of distilled water. An orange precipitate immediately formed. This was separated by filtration, successively extracted with petroleum ether and ethanol, and dried *in vacuo* at 80°C for 24 h.

IR (KBr), ν_{max}, cm^{-1}: 3451vw, 3368vw, 3219vw, 3067vw, 3040vw, 3001vw, 2959w, 2883w, 2837vw, 1682w, 1626m, 1595vs, 1572vs, 1508s, 1483s, 1443m, 1416s, 1385m, 1369w, 1304m, 1290m, 1254s, 1198m, 1161vs, 1063s, 1034s, 1011s, 962m, 887w, 843s, 804s, 748m, 721m, 708m, 683m, 648w. Far-IR [ν (KBr, cm^{-1})]: 631vw, 606vw, 571m, 544s, 444vw, 399vw, 388w, 365vw, 341w, 330w, 253w, 230m, 216vs, 198s, 189m. ^{1}H-NMR (DMSO-d_6, 400.13 MHz, δ, ppm): 8.62 (—CH=N—), 8.56

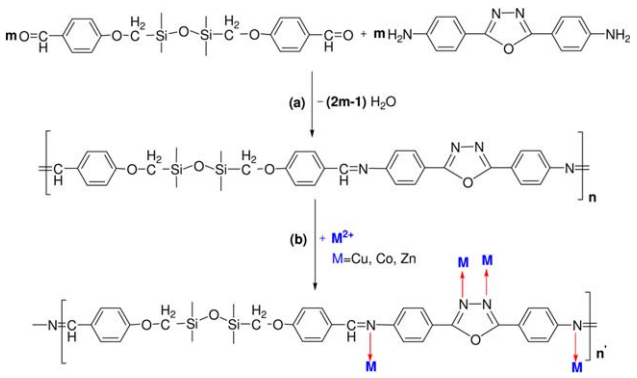

Scheme 1. Synthetic routes for the preparation of (a) PAZ2 and (b) its metal complexes. [Color figure can be viewed in the online issue, which is available at wileyonlinelibrary.com.]

(—CH═N—), 8.15–6.71 (aromatic protons from diamine and dialdehyde), 3.87–3.68 (—CH_2—), 0.24–0.07 (—Si—CH_3). GPC results: number-average molecular weight (M_n) = 4350 g/mol, Polydispersity index (PDI) = Weight-average molecular weight (M_w)/M_n = 1.6

Synthesis of PAZ2–M, where M = Cu (PAZ2-Cu), Co (PAZ2-Co), or Zn (PAZ2-Zn). PAZ2-Cu 2,5-Bis(*p*-aminophenyl)−1,3,4-oxadiazole (0.252 g, 1 mmol) in DMF (5 mL) was added to a solution of bis(formyl-*p*-phenoxymethyl) tetramethyldisiloxane (0.404 g, 1 mmol) dissolved in $CHCl_3$ (5 mL), and the mixture was stirred to reflux for 8 h. The resulting polymer solution was then added stepwise to a solution of $CuCl_2 \cdot 2H_2O$ (0.682 g, 4 mmol) in a methanol/$CHCl_3$ solvent mixture (5 mL). The color changed to dark green. A few drops of triethylamine were added to the solution, and the mixture was heated at 60°C for 2 h. After the evaporation of the solvents at room temperature, the resulting dark green crystalline powder was thoroughly washed with water and dried under high vacuum.

IR (KBr), ν_{max}, cm^{-1}: 3308w, 3225w, 3119w, 3069w, 2959w, 2899vw, 1686s, 1649s, 1599vs, 1578s, 1506s, 1495s, 1435m, 1416m, 1385m, 1371m, 1302m, 1292m, 1258s, 1173s, 1159s, 1067s, 1040s, 964m, 841vs, 804s, 744m, 721w, 704m, 683m, 650w, 635w. Far-IR (ν_{max}, KBr, cm^{-1}): 608s, 559s, 538s, 515s, 424w, 399w, 370w, 330w, 299m, 280m, 243vs, 235vs, 231vs, 226s, 216vs. XRF: Cu/Si molar ratio = 1:2. GPC results: M_n = 5350 g/mol, PDI = M_w/M_n = 1.1.

The same methods were applied to obtain PAZ2–Co and PAZ2–Zn.

PAZ2-Co was obtained similarly, as a green powder.

IR (KBr), ν_{max}, cm^{-1}: 3549s, 3412s, 2959w, 1651s, 1599vs, 1508s, 1495s, 1437m, 1414m, 1383m, 1375m, 1342w, 1306m, 1258s, 1171s, 1036s, 1013s, 841s, 804s, 744m, 723m, 702m, 650w. Far-IR (ν_{max}, KBr, cm^{-1}): 638m, 625w, 608m, 567s, 534vs, 517vs, 413m, 363m, 326m, 303m. XRF: Co/Si molar ratio = 1:1. GPC results: M_n = 3050 g/mol, PDI = M_w/M_n = 1.1.

PAZ2-Zn was obtained similarly, as an orange–yellow powder.

IR (KBr), ν_{max}, cm^{-1}: 3443w, 3354w, 3223vw, 2959m, 2934w, 2839vw, 1655vs, 1597vs, 1574vs, 1508s, 1493s, 1437m, 1418m, 1383s, 1304m, 1292m, 1254s, 1167s, 1034s, 964m, 883w, 837vs, 802s, 748m, 721m, 706m, 689m, 650w. Far-IR (ν_{max}, KBr, cm^{-1}): 608w, 571w, 546m, 513w, 426vw, 384w, 332w, 299vw, 226m, 214vs. XRF: Zn/Si molar ratio = 1:2. GPC results: M_n = 2800 g/mol, PDI = M_w/M_n = 1.1.

RESULTS AND DISCUSSION

Synthesis and Characterization of the New Compounds

Bis(formyl-*p*-phenoxymethyl) tetramethyldisiloxane prepared according to our previously established procedure[32] was reacted with 2,5-bis(*p*-aminophenyl)-1,3,4-oxadiazole in a 1:1 molar ratio in a $CHCl_3$/DMF solvent mixture to obtain the corresponding PAZ2 [Scheme 1(a)]. The dialdehyde contained a highly flexible tetramethyldisiloxane segment, which was expected to induce increased solubility, whereas the diamine was chosen as a photoactive component.[34–36]

The formation of PAZ2 was initially verified by FTIR spectroscopy (Figure 1S, Supporting Information), and the main data of the spectra are summarized in Table I. The structure was confirmed by the disappearance of the specific absorption bands of

Table I. FTIR Analysis Results for the PAZ2 and the Derived Metal Complexes

	Wave number (cm^{-1})							
Sample	CH═N	C═N (imidazole ring)	C═C (aromatic)	— CH_2—O—Ar—	Si—O—Si	Si—CH_3	Oxadiazole ring	M—N
PAZ2	1626	1595	1572, 843	1034	1063	1254, 804	962, 1011, 1098 (sh)[a]	—
PAZ2-Cu	1649	1599	1578, 841	1040	1067	1258, 804	964, 1013 (sh)[a]	424, 370
PAZ2-Co	1651	1599	1572 (sh),[a] 841	1036	1068 (sh)[a]	1258, 804	963 (sh),[a] 1013	413
PAZ2-Zn	1655	1597	1574, 837	1034	1063 (sh)[a]	1254, 802	964, 1013 (sh)[a]	417 (sh),[a] 384

[a] Spectral details visible in the IR spectra are provided in the Supporting Information (Figures 3S–7S).

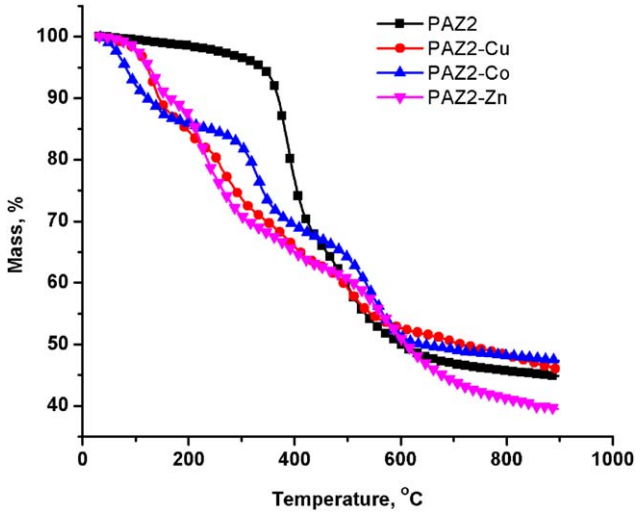

Figure 1. TGA curves for PAZ2 and PAZ2–metal complexes. [Color figure can be viewed in the online issue, which is available at wileyonlinelibrary.com.]

the carbonyl and amine groups around 1690 cm^{-1} (carbonyl) and 3321 and 3202 cm^{-1} (primary amine groups), respectively, and the presence of the characteristic band at 1626 cm^{-1} for newly formed imine groups.

The ^{1}H-NMR spectrum of PAZ2 (Figure 2S, Supporting Information) revealed the presence of the following signals: 8.56–8.62 ppm (—C*H*═N—), 6.71–8.15 ppm (protons from aromatic rings derived from the two comonomers), 3.70–3.87 ppm (—C*H*$_2$—O—), and 0.07–0.24 ppm (Si—C*H*$_3$). The presence of these signals and their intensity ratios, —C*H*$_3$/—C*H*$_2$—:*H* aromatic/—C*H*═N— = 6:2:8:1, confirmed the presumed structure.

The reaction product was partly soluble in $CHCl_3$ and completely soluble in polar solvents, such as DMF and DMSO. The solubility was especially due to the flexible tetramethyldisiloxane units[22] and the presence of kinking etheric functions[18] and heterocyclic units that disrupted the packaging chain.[35,41]

GPC measurements in DMF revealed a unimodal curve and permitted us to estimate the molecular mass values, which were M_n = 4350 g/mol, M_w = 6960 g/mol, and PDI = 1.6.

The presence of nitrogen atoms in the azomethine and oxadiazole groups provided us with the possibility of preparing metal complexes through the treatment of the obtained PAZ2 with transition metals. Copper, cobalt, and zinc salts were used to this aim. Two strategies could be used for the synthesis of metal complexes of the PAZ2. One of them is the stepwise synthesis, including the preparation of Schiff bases, separation, and full characterization followed by their utilization as ligands for coordination to metal ions. The other one was the assembly of the Schiff-base ligands from the starting materials in the presence of metal ions (*in situ* or with the template methodology). In this study, we used a modified two-step procedure, where the PAZ2 was prepared and added directly (without being isolated) over the metallic salt solution. The complexation reaction was led with a high salt excess in the presence of triethylamine in a 1:1 v/v $CH_3OH/CHCl_3$ solvent mixture [Scheme 1(b)].

The accomplishment of the complexation reactions was initially proven by modifications that appeared in the FTIR spectra (Figures 3S–5S, Supporting Information). The absorption band at 1626 cm^{-1} assigned to the CH═N group in PAZ2 shifted to

Table II. Main Parameters of the Thermograms

Compound	Decomposition stage	*T* (°C)			Weight loss (%)[a]	Residue, at 900°C (%)
		T_{on}	T_{max}	T_{off}		
PAZ2	I	345	388	464	31.97	46.12
	II	464	497	800	21.90	
PAZ2-Cu	I	30	133	187	13.00	45.87
	II	187	204	250	4.99	
	III	250	256	365	11.50	
	IV	365	390	413	7.37	
	V	413	499	800	17.20	
PAZ2-Co	I	30	79	154	13.95	47.32
	II	154	332	353	16.94	
	III	353	548	800	21.36	
PAZ2-Zn	I	30	142	152	10.33	39.43
	II	152	225	363	20.16	
	III	363	389	407	6.87	
	IV	407	565	800	22.76	

T_{on}, temperature of thermal degradation onset; T_{max}, temperature corresponding to the maximum rate of decomposition for each stage evaluated from the peaks of DTG curves; T_{off}, final thermal degradation temperature.
[a] Weight loss corresponding to the T_{max} values.

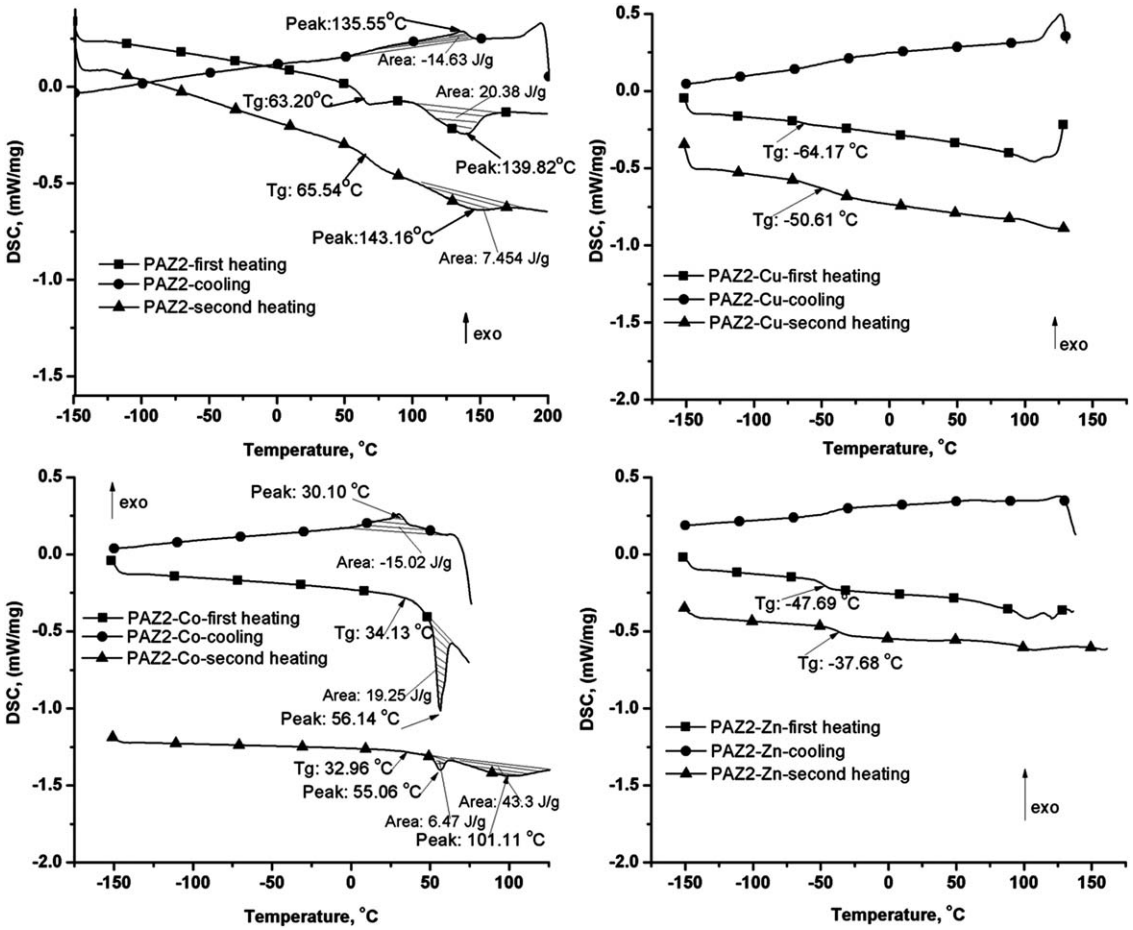

Figure 2. DSC curves for PAZ2 and its metal complexes.

higher wave numbers by 25–35 cm^{-1} in the metal complexes (Table I and Figure 3S, Supporting Information), and this indicated the participation of the azomethine nitrogen atoms in the complexation reaction.[42–45]

In the far-IR region, the characteristic vibrations for the newly created M—N coordination bonds can be seen at 424 and 370 cm^{-1} (Cu—N), 413 cm^{-1} (Co—N), and 384 and 417 cm^{-1} (Zn—N)[46–48] (Figure 6S, Supporting Information). In addition, those assigned to M—Cl (330 and 243 cm^{-1} for PAZ2–Cu, 326 and 303 cm^{-1} for PAZ2–Co, and 332 cm^{-1} for PAZ2–Zn; Figure 8S, Supporting Information) were observed.

Analysis by XRF revealed different M/Si molar ratios in the three complexes: Cu/Si = 1:2, Co/Si = 1:1, and Zn/Si = 1:2. This difference was attributed to the different affinities of the three metals for the ligating groups and their coordination pattern.

Evaluation of the Properties

Thermal Behavior. The thermostabilities of the PAZ2 and its metal complexes were evaluated by thermogravimetric analysis (TGA) in a nitrogen atmosphere; the TGA and derivative thermogravimetric (DTG) curves are comparatively presented in Figures 1 and 8S (Supporting Information). Some characteristics extracted from these curves are presented in Table II.

As shown, PAZ2 had a good thermal stability, with its decomposition starting around 345°C. This could have been due to the presence of *p*-substituted phenylene rings, which are known for their thermal stability,[49] but also to the presence of noncovalent interactions: interchain hydrogen bonds between azomethine linkages (—HC═N—) and oxygen atoms from oxadiazole rings and π–π stacking interactions between aromatic rings. Its thermal decomposition occurred in two steps. According to the literature,[49,50] the azomethine groups were broken first;[50] this was followed by the degradation of the ether linkage and *p*-substituted phenylene rings.[49] The decomposition of the metal complexes began very early, at much lower temperatures than that corresponding to PAZ2, and is more complicated (Table II). The first stage of degradation was observed between 30 and 200°C. This may have been due to the loss of residual solvent and coordinated water molecules. After 200°C, a gradual mass loss was observed in the following stages of degradation when the breaking of azomethine bonds and the decomposition of *p*-substituted phenylene rings can occur. There are many factors that may contribute to the reduction of thermal stability of the resulted metal complexes: the bulkiness of the metals, the coordination mode, the number of the coordinative bonds, the solvent and contra-ion nature.[33,51] These factors produce disruptions in the packing structure of the PAZ2 by involving of both nitrogen atoms (from imine groups and oxadiazole

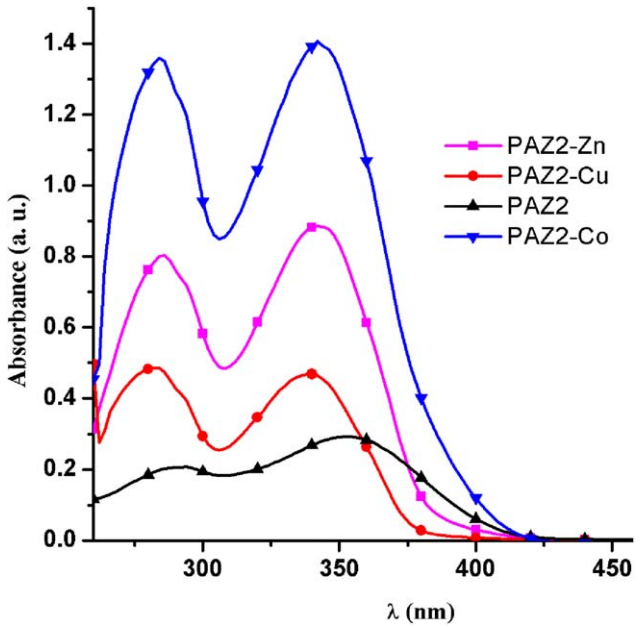

Figure 3. Electronic absorption spectra of siloxane PAZ2 and its metal complexes in DMSO. [Color figure can be viewed in the online issue, which is available at wileyonlinelibrary.com.]

ring) in complexation of metal ions.[33] The lower thermostability of metal complexes as compared with the corresponding ligands is also reported in literature.[52–54] It seems that the presence of the metal catalyzes the early initiation of the complex decomposition. The char yield at 900°C was between 39 and 46% for the PAZ2 complexes.

The DSC traces (second heating run) revealed the presence of glass transitions for PAZ2 and its metal complexes; this is a characteristic of polymeric materials (Figure 2 and Table IS). Thus, the PAZ2 showed a glass transition at 65.54°C and a melting temperature peak centered at 139.82°C in the first run. In the second run, the melting process was much diminished; the enthalpy was 7.454 J/g as compared with 20.380 J/g in the first heating cycle, whereas the peak shifted to 143.16°C. We assumed that the initial degree of organization could not be reached during cooling under the experimental conditions.

In the first heating run, the Co complex exhibited a sharp melting peak at 56.14°C (enthalpy = 19.25 J/g). Above this temperature, as TGA showed, the complex decomposed. Therefore, in another experiment, a fresh sample was heated in the temperature range of −150 to 57°C, to prevent decomposition. With subsequent cooling, the crystallization was observed at 30.10°C. In the second heating process, both the glass-transition temperature (T_g) and melting temperatures were recorded at 32.96 and 55.06°C, respectively, but the melting enthalpy (6.47 J/g) was much reduced compared to the one registered in the first run (19.25 J/g); this was similar to the case of PAZ2. The Cu and Zn metal complexes showed lower T_g values compared with those of the PAZ2 and the Co complex at −50.61 and −37.68°C, respectively, whereas the melting process was not well-evidenced. We inferred that the melting was affected by the decomposition, as observed from TGA. The fact that PAZ2Co showed a much IR (KBr), n_{max}, cm^{-1}: higher glass transition

Table III. Summary of Ultraviolet–Visible and Emission Characteristics

Sample	λ_{max} (nm)[a]	λ_{em} (nm)[b]	$\Delta\nu$ (cm^{-1})[c]	Eg[d]
PAZ2	354; 294	406.5	3648	3.01
PAZ2–Cu	340; 284	405.6	4757	3.16
PAZ2–Co	342; 284	405.3	4566	3.20
PAZ2–Zn	342; 284	404.9	4542	3.19

[a] wavelength in the absorption maximum.
[b] wavelength in the emission maximum.
[c] $\Delta\nu$, Stokes shift. $\Delta\nu = \nu_{abs} - \nu_{em}$, with ν_{max} and ν_{em}: wavenumber in absorption and emission maximum, respectively.
[d] Calculated from relation $E_g = 1240/\lambda_{max}$.

than PAZ2–Cu and PAZ2–Zn might be explained by the XRF data, which indicated a higher (double) metal content in PAZ2-Co compared to the other complexes. The higher density of the metal in the coordination points led to the chain stiffening and, thus, to higher T_g.

Absorption and Photoluminescence Properties. The electronic absorption spectra of PAZ2 in the DMSO solution exhibited two absorption bands at about 296 and 354 nm, respectively (Figure 3). The long-wave absorption band resulted from a π–π^* transition involving the azomethine–phenyl–oxadiazole system.[35] The starting oxadiazole compound, 2,5-bis(*p*-aminophenyl)-1,3,4-oxadiazole, presented two absorption maxima located at 286 and 342 nm in DMSO solution. The spectral shift to longer wavelengths of the PAZ2 absorption band in comparison with the oxadiazole derivative was determined by the enhanced conjugation in the polymer chain.

The complexes of PAZ2 with Cu^{2+}, Co^{2+}, and Zn^{2+} as metal ions showed absorption bands around 340 and 286 nm, respectively, in DMSO (Table III). As shown in Figure 3, the electronic absorption spectra of PAZ2 complexes were blueshifted compared to that of PAZ2 because of the formation of azomethine complexes.[33] The energy band-gap values (E_g) calculated from the absorption spectra for the PAZ2 derivatives were situated in the range 3.0–3.2 eV and close to the values of silane-containing polyazomethine.[33]

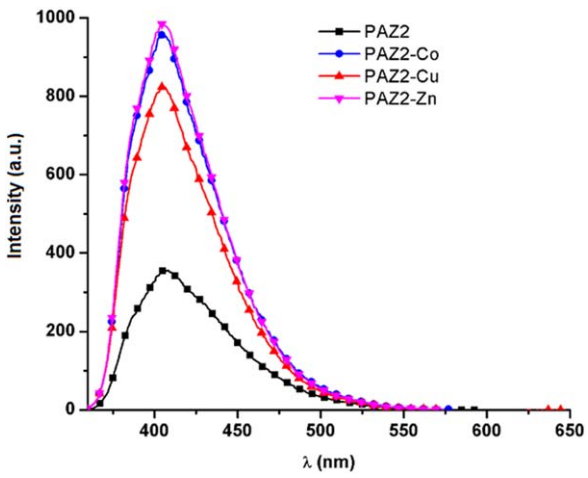

Figure 4. Fluorescence spectra of PAZ2 and its complexes. [Color figure can be viewed in the online issue, which is available at wileyonlinelibrary.com.]

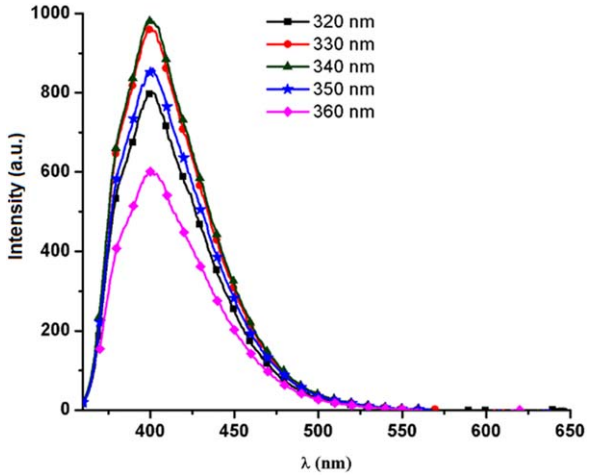

Figure 5. Emission spectra of PAZ2–Zn at different excitation wavelengths. [Color figure can be viewed in the online issue, which is available at wileyonlinelibrary.com.]

The light-emitting characteristics of the siloxane-containing PAZ2 derivatives were analyzed with fluorescence spectra. Figure 4 depicts the emission spectra of PAZ2 and its complexes in DMSO solution. Upon excitation (wavelength = 340 nm), PAZ2 and its metal complexes displayed an emission band around 405 nm. An enhancement of fluorescence was observed by the coordination of PAZ2 with metal ions. The Zn and Co complexes of PAZ2 showed similar intense emission maxima when excited at 340 nm. The enhancement of fluorescence was attributed to the involvement of donor groups of the PAZ2 in the metal complex formation; this caused increases in the planarity and rigidity of the polymer chain and, hence, the decrease of the nonradiative decay of the excited state.[55]

The same emission pattern was also observed for PAZ2 with DMF as a solvent. Generally, the shape of the emission bands was not symmetrical, and a tail toward longer wavelengths was evidenced. In all cases, the polymer solutions emitted violet–blue light under excitation at 340 nm.

The emission spectra of the PAZ2–Zn in DMF solution at several excitation wavelengths are shown in Figure 5. The independence of the emission spectra of the excitation wavelength and the fact that the fluorescence spectra were not affected in shape by the excitation wavelength indicated the presence of a single excited emission species in the polymer main chain. The highest emissions were obtained when the PAZ2 complex was excited at 340 and 330 nm, respectively.

The calculated Stokes shift values were higher for the PAZ2 complexes compared with that of PAZ2 (Table III). These values of the Stokes shifts evidenced some differences in the energy loss; this took place during the transition from S_0 (ground state) to S_1 (singlet excited state). The emission intensities of the PAZ2 complexes were lower than those of the complexes of silane-containing polyazomethine because of the effect of the σ-electron delocalization of the silane unit along the polymer chain.[33,56]

Because the PAZ2s possessed basic nitrogen atoms, which represent receptors for protons, the optical properties of these polymers should have been modified by protonation. Indeed, upon the gradual addition of trifluoroacetic acid (TFA), a decrease in the absorption at 354 nm accompanied by an increase in the intensity of the absorption band around 294 nm occurred compared to the pristine polymer. Concomitantly, a blueshift of the two absorption bands was observed. Specifically, the absorption band at 354 nm for PAZ2 shifted to 340 nm, and the other band around 294 was shifted to 284 nm by protonation. The hypsochromic shift of the absorption bands were due to the formation of some shorter conjugation units in the polymer chain by protonation.[57] Similar results were obtained for PAZ2-Cu complex, but a lower blueshift was found because of protonation. Upon TFA addition, the emission of PAZ2 showed a significant enhancement in the intensity (up to threefold) when 0.5 mEq of TFA was added (Figure 6). The addition of increasing amounts of TFA led to the progressive decrease in the emission intensity at 406.5 nm. Finally, by the addition of 8.6 mEq of TFA, the emission intensity of PAZ2 was twice as big as the pristine polymer (Figure 6). During the addition of TFA, the emission maximum remained unshifted. After 10 days, the emission spectrum of PAZ2 for 8.6 mEq of TFA addition was not changed. The same emission pattern was found for PAZ2-Cu, but in this case, a 1.5-fold increase of the emission intensity was observed.

Dielectric Measurements. By the dielectric relaxation spectroscopy method, complex dielectric permittivity [$\varepsilon^*(f) = \varepsilon'(f) + i\varepsilon''(f)$], with f - measurement frequency and i - the imaginary unit, was measured isothermally. In Figure 7, the temperature and frequency dependencies of the dielectric constant (ε') and dielectric loss (ε'') are represented, that is, the real and the imaginary part of ε^*, respectively. Examination of these results revealed the existence of

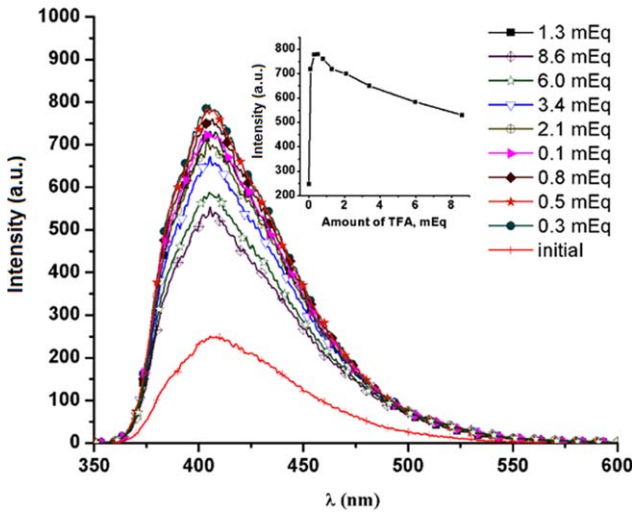

Figure 6. Emission spectra of PAZ2 upon the addition of different equivalents of TFA in a DMSO solution (excitation wavelength, $\lambda_{ex} = 340$ nm). The inset shows a plot of the emission intensity at 406.5 nm versus the amount of TFA. [Color figure can be viewed in the online issue, which is available at wileyonlinelibrary.com.]

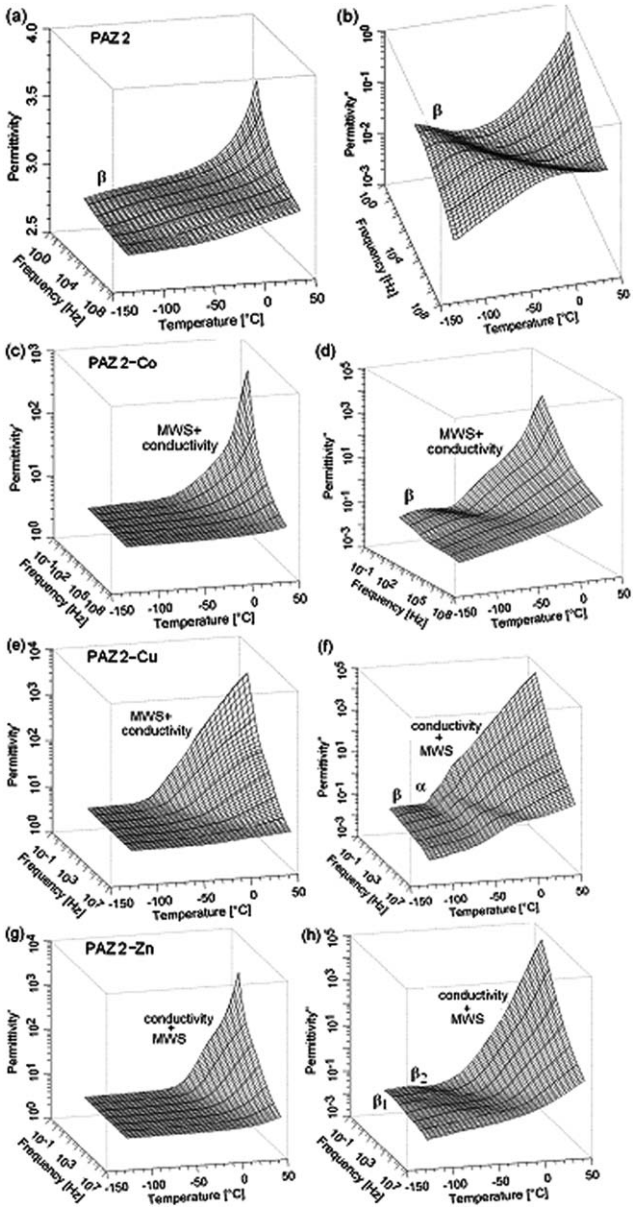

Figure 7. Frequency and temperature dependence of ε' and ε'' for (a,b) PAZ2, (c,d) PAZ2–Co, (e,f) PAZ2–Cu, and (g,h) PAZ2–Zn.

dipolar relaxations and conductivity (σ) contributions at higher temperatures. Depending on the temperature region where the relaxations appeared and in concordance with the DSC data, they were assigned to different molecular movements. So, at temperatures below the calorimetric glass transition, there were β relaxations corresponding to local movements of the chain segments and, in the case of PAZ2–Cu, at temperatures slightly higher than T_g, to α relaxation assigned to segmental movement responsible for the glass transition. Because of the increased σ at higher temperatures, an α relaxation correlating well with the DSC glass transition was observed only for the polymer with the lowest T_g. The dipolar relaxations noted in Figure 7 were observed as peaks on ε'' and a step increase on the ε' representations, which shifted to higher temperatures with increasing frequency. Dipolar relaxations were observed well on ε' curve only for PAZ2. For the PAZ2–metal complexes, especially at lower frequencies, there was a steep increase of ε' at positive temperatures, which was caused by the space charge polarization phenomena.[58] In this case, the rise in the permittivity at low frequencies was a result of electrode polarization effects,[59] space charge effects observed in ionic glasses,[60] and also trace quantities of water that may have been retained in the samples.[59] The exponential increase in ε'' in the same temperature range was also caused by the increased σ.

In both representations, there was a deviation from the monotonous increases in ε' and ε'' in logarithmic scale. This frequency-dependent shoulder, especially at low frequencies, may come from the separation of charges at interfaces.[61] The effect, called the *Maxwell–Wagner–Sillars polarization*, occurred either at the inner dielectric boundary layers on a mesoscopic scale, for example, between amorphous and crystalline regions, or at the external electrode–sample interface on a macroscopic scale. At high frequencies, the ions could not diffuse in the direction of electric field, and the values of ε' and ε'' decreased.[62] In the case of the PAZ2 complexes, some dipolar relaxation processes that could occur at higher temperatures were obscured by the observed large σ contributions.

Compared to the PAZ2, its derived metal complexes presented β relaxation at slightly higher temperatures for the same frequency, as illustrated in Figure 8 by the replot of the ε'' data recorded isothermally against the temperature for 10 Hz. For the PAZ2–Zn complex, this relaxation was followed by a β_2 process with a small amplitude and more slowly compared to β_1. The displacement of β to higher temperatures indicated a slower process, probably because crosslinking caused by metal complex formation reduced the local mobility.

For dipolar relaxations, each isothermal relaxation peak from the frequency sweep [$\varepsilon''(f)$] was analyzed through fitting to the Havriliak–Negami (HN) expression:[63]

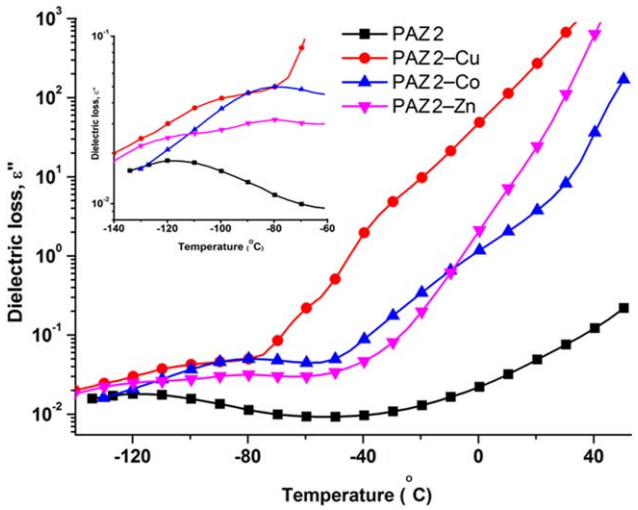

Figure 8. Variation of ε'' with the temperature at 10 Hz for PAZ2 and the resulting metal complexes PAZ2–Cu, PAZ2–Co, and PAZ2–Zn. The inset shows a magnification of the β-relaxation region. [Color figure can be viewed in the online issue, which is available at wileyonlinelibrary.com.]

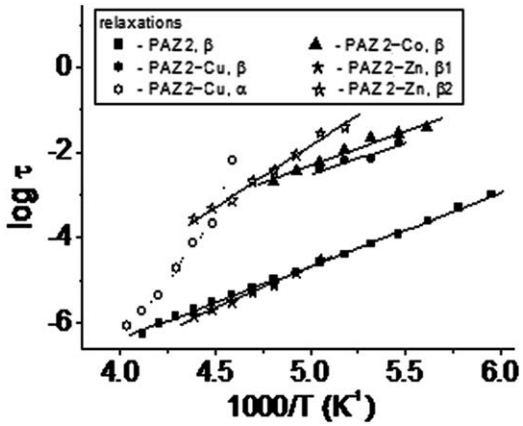

Figure 9. Activation Arrhenius maps of log τ versus $1/T$.

$$\varepsilon'' = \mathrm{Im}\left(\varepsilon_u + \frac{\varepsilon_r - \varepsilon_u}{[1+(i\omega\tau)^a]^b}\right)$$

where $\Delta\varepsilon = \varepsilon_r - \varepsilon_u$ represents the dielectric strength (where ε_r and ε_u represent the relaxed and unrelaxed values of ε' for each relaxation), $\omega = 2\pi f$ is the angular frequency, a and b represent shape parameters that characterize the width and the asymmetry of the loss curves, and τ is the relaxation time for each process.[61] For the overlapped relaxations β_1 and β_2, the $\varepsilon''(f)$ spectra were fitted to a sum of two HN functions, and for a considerable σ contribution at higher temperatures and lower frequencies, an additional exponential term ($k\omega^{-s}$, where k is a constant) was added.

In the case of local relaxation, the obtained τ values obeyed Arrhenius law (Figure 9):

$$\tau = \tau_0 \exp\left(E_a/kT\right)$$

where E_a is the apparent activation energy of the process, k is Boltzmann's constant, T is temperature (K) and τ_0 is a the preexponential factor and represents the relaxation time at very high temperature. In Table IV, the values of activation energies obtained for β relaxations are shown.

Regarding the α relaxation observed for PAZ2–Cu, once the temperature decreased close to T_g, τ increased rapidly (Figure 9), as is typical incooperative relaxations. This behavior represented another confirmation that the process was assigned to the dynamic glass transition. In this case, the τ values were described well by the Vogel–Fulcher–Tamman–Hesse equation:[64]

Table IV. Arrhenius Parameters for Local Relaxations

Sample	Relaxation	E_a (kJ/mol)	τ_0 (s)
PAZ2	β	32.86	5.84×10^{-14}
PAZ2-Cu	β	27.25	2.5×10^{-10}
PAZ2-Co	β	29.67	9.4×10^{-11}
PAZ2-Zn	$\beta 1$	38.02	2.6×10^{-15}
	$\beta 2$	55.30	5.4×10^{-17}

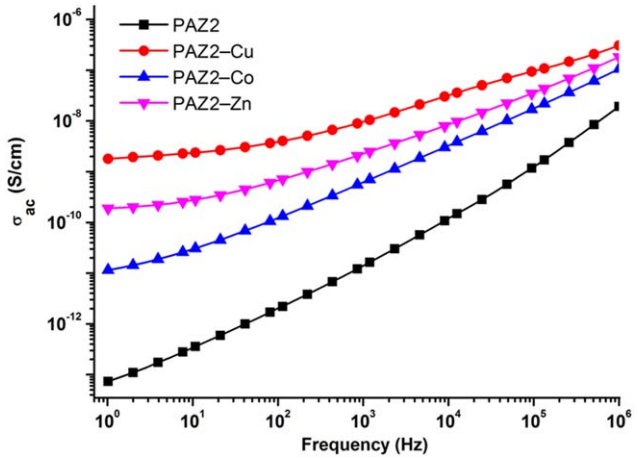

Figure 10. Frequency dependence of σ_{ac} for PAZ2 and its metal complexes at 25°C. [Color figure can be viewed in the online issue, which is available at wileyonlinelibrary.com.]

$$\tau = \tau_0 \exp\left[B/k(T - T_0)\right]$$

with the fitting parameters $\tau_0 = 1.5 \times 10^{-13}$ s, $B = 0.11$ eV, and $T_0 = 167$ K (B and T_0 being constants). Furthermore, the change in σ due to metal complexation was followed. The alternating-current conductivity (σ_{ac}) values were evaluated from the ε'' data with the following relation:[65]

$$\sigma_{ac}(\omega) = \varepsilon_0 \omega \varepsilon''$$

where ε_0 is the permittivity of free space. The temperature dependence of σ at several frequencies is shown in Figure 9S (Supporting Information). At a constant temperature, σ_{ac} showed dispersion with almost 10 orders of magnitude with increasing frequency, as is common in heterogeneous and disordered solids.[66] In the case of PAZ2, σ increased slightly at positive temperature only for the lowest frequencies; for 10 Hz, it remained on the order of magnitude of 10^{-13} S/cm, whereas at a higher frequency, it did not vary much up to 50°C, as commonly observed for insulators. In contrast, for the lowest frequency, the PAZ2 derivatives presented an increase of σ_{ac} up to 10 orders of magnitude for PAZ2–Cu and PAZ2–Zn and 4 orders of magnitude for PAZ2–Co with increasing temperature. Also, for complexes, the significant increase in σ_{ac} started at lower temperatures, around −80°C for PAZ2–Cu and −50°C for PAZ2–Co and PAZ2–Zn.

Figure 10 shows the variation of σ_{ac} with the frequency at 25°C. For PAZ2, σ_{ac} increased approximately linearly in double logarithmic scale, whereas the metal complexes presented a plateau region at low frequencies; this corresponded to direct-current conductivity (σ_{dc}).[65] In this case, σ_{ac} is given by the following expression:[67]

$$\sigma = \sigma_{dc} + \sigma_{ac}\omega^s$$

where σ_{dc} is the frequency-independent term and ω^s is the Jonscher term.[68] In the frequency domain corresponding to the plateau region and lower, the charge carriers jumped over long distances; this allowed electric conduction throughout the entire volume of the sample, and the conductivity corresponded to

σ_{dc}. At the lowest frequency, PAZ2 presented a very low conductivity, approximatively 10^{-14} (S/cm), but it grew to 10^{-11} (S/cm) for polychelates with Co, 10^{-10} (S/cm) for PAZ2–Zn, and 10^{-9} (S/cm) for PAZ2–Cu. These values were still low compared, for example, to network polymer electrolytes based on polysiloxane with σ_{dc} on the order of 10^{-5} to 10^{-4} (S/cm). In our case, the conductivity was too low for the systems to be used as polymer electrolytes, but they are interesting for other applications, for example, in sensors.

CONCLUSIONS

A dialdehyde-containing highly flexible tetramethyldisiloxane fragment, bis(formyl-*p*-phenoxymethyl) tetramethyldisiloxane, and an N-rich diamine containing the oxadiazole ring were used to build a new PAZ2 of relative low molecular mass ($M_n = 4350$ g·mol^{-1}). Its structure was confirmed through FTIR and ^{1}H-NMR spectroscopies. By subsequent reactions with various metal salts under the same conditions, metal complexes were obtained with different metal contents, as determined by energy-dispersive X-ray fluorescence. This was likely due to the different coordination pattern, which depended on the nature of the metal. The TGA revealed the diminished thermal stability of the PAZ2–metal complexes as compared to that of the ligand. The identification of the glass transitions on the DSC curves supported the polymeric nature of the compounds. The electronic absorption spectra of the PAZ2 complexes were blueshifted compared to the ligand. The light-emitting characteristics of the PAZ2 derivatives were analyzed with the fluorescence spectra. The calculated Stokes shift values were higher for the PAZ2 complexes compared with that of PAZ2. The presence of basic nitrogen atoms along the chain led to the sensitive change in the optical properties under the acid conditions because of protonation. Thus, an increase in the light emission intensities occurred concomitantly with a blueshift of the absorptions in the presence of TFA. Dielectric spectra at various frequencies and temperatures revealed the existence of β relaxations assigned to local movements of the polymer chain. Compared to PAZ2, its derived metal complexes presented slower β relaxation processes; this was probably due to the crosslinking caused by metal complex formation, and this reduced the local mobility.

ACKNOWLEDGMENTS

This work was supported by a grant of the Ministry of National Education, CNCS – UEFISCDI, project number PN-II-ID-PCE-2012-4-0261. The authors sincerely thank C. D. Varganici (Centre of Advanced Research in Bionanoconjugates and Biopolymers) for the registration of the TG and DSC curves.

REFERENCES

1. Leung, A. C. W.; MacLachian, M. J. *J. Inorg. Organomet. Polym. Mater.* **2007**, *17*, 57; and references therein.
2. Naka, K.; Horii, E.; Chujo, Y. *Polym. J.* **2000**, *32*, 316.
3. Kaya, I.; Koyuncu, S. *Iran. Polym. J.* **2007**, *16*, 261.
4. Cazacu, M.; Marcu, M.; Vlad, A.; Toth, A.; Racles, C. *J. Polym. Sci. Part A: Polym. Chem.* **2003**, *41*, 3169.
5. Kaliyappan, T.; Kannan, P. *Prog. Polym. Sci.* **2000**, *25*, 343.
6. Marcu, M.; Cazacu, M.; Vlad, A.; Racles, C. *Appl. Organomet. Chem.* **2003**, *17*, 693.
7. Cazacu, M.; Marcu, M.; Vlad, A.; Rusu, G. I.; Avadanei, M. *J. Organomet. Chem.* **2004**, *689*, 3005.
8. Cazacu, M.; Marcu, M.; Vlad, A.; Vasiliu, M. *J. Macromol. Sci. Chem.* **2004**, *41*, 565.
9. Vasiliu, M.; Cazacu, M.; Marcu, M.; Racles, C.; Vlad, A. *Appl. Organomet. Chem.* **2005**, *19*, 614.
10. Cazacu, M.; Vlad, A.; Munteanu, G.; Airinei, A. *J. Polym. Sci. Part A: Polym. Chem.* **2008**, *46*, 1862.
11. Vlad, A.; Cazacu, M.; Munteanu, G.; Airinei, A.; Budrugeac, P. *Eur. Polym. J.* **2008**, *44*, 2668.
12. Kaliyappan, T.; Kalman, P. *Iran. J. Polym. Sci. Technol.* **1995**, *4*, 18.
13. Prakash, A.; Adhikari, D. *Int. J. Chem. Tech. Res.* **2011**, *3*, 1891.
14. Catanescu, O.; Grigoras, M.; Colotin, G.; Dobreanu, A.; Hurduc, N.; Simionescu, C. I. *Eur. Polym. J.* **2001**, *37*, 2213.
15. Saraii, M.; Entezami, A. A. *Iran. Polym. J.* **2003**, *12*, 43.
16. Vacareanu, L.; Ivan, T.; Grigoras, M. *High Perform. Polym.* **2012**, *24*, 717.
17. Marin, L.; Cozan, V.; Bruma, M. *Polym. Adv. Technol.* **2006**, *17*, 664.
18. Marin, L.; Cozan, V. *Memories Sci. Sect. Romanian Acad. Ser. IV* **2010**, *33*, 35.
19. More, A. S.; Sane, P. S.; Patil, A. S.; Wadgaonkar, P. P. *Polym. Degrad. Stab.* **2010**, *95*, 1727.
20. Jung, S. H.; Lee, T. W.; Kim, Y. C.; Suh, D. H.; Cho, H. N. *Opt. Mater.* **2002**, *21*, 169.
21. Farcas, A.; Harabagiu, V. *Rev. Roum. Chim.* **2007**, *52*, 887.
22. Iwan, A.; Schab-Balcerzak, E.; Pociecha, D.; Krompiec, M.; Grucela, M.; Bilski, P.; Klosowski, M.; Janeczek, H. *Opt. Mater.* **2011**, *34*, 61.
23. Bian, L. J.; Yang, X. Y. *Makromol. Chem. Macromol. Symp.* **1991**, *47*, 357.
24. Palewicz, M.; Iwan, A.; Sibinski, M.; Sikora, A.; Mazurek, B. *Energy Procedia* **2011**, *3*, 84.
25. Racles, C.; Cazacu, M.; Vasiliu, M.; Cozan, V. *Polym. Plast. Technol. Eng.* **2005**, *44*, 1049.
26. Shin, K.; Aoki, T.; Oikawa, E. *Macromol. Rapid Commun.* **1995**, *16*, 599.
27. Bronnikov, S.; Racles, C.; Cozan, V. *Liq. Cryst.* **2009**, *36*, 1366.
28. Bronnikov, S.; Nasonov, A.; Racles, C.; Cozan, V. *Soft Matter* **2008**, *6*, 119.
29. Bronnikov, S.; Racles, C.; Nasonov, A.; Cazacu, M. *Liq. Cryst.* **2006**, *33*, 1015.
30. Racles, C.; Cozan, V.; Sajo, I. *High Perform. Polym.* **2007**, *19*, 541.
31. Racles, C.; Cozan, V. *High Perform. Polym.* **2002**, *14*, 169.
32. Racles, C.; Cozan, V.; Cazacu, M.; Foldes, E.; Sajo, I. *High Perform. Polym.* **2002**, *14*, 397.

33. Zaltariov, M. F.; Cazacu, M.; Shova, S.; Varganici, C. D.; Vacareanu, L.; Musteata, V.; Airinei, A. *Des. Monomers Polym.* **2014**, *17*, 668.
34. Marin, L.; Damaceanu, M. D.; Timpu, D. *Soft Matter* **2009**, *7*, 1.
35. Marin, L.; Perju, E.; Damaceanu, M. D. *Eur. Polym. J.* **2011**, *47*, 1284.
36. Chen, Z.; Ding, F.; Hao, F.; Guan, M.; Bian, Z.; Ding, B.; Huang, C. *New J. Chem.* **2010**, *34*, 487.
37. Hamciuc, E.; Hamciuc, C.; Bruma, M.; Schulz, B. *Eur. Polym. J.* **2005**, *41*, 2989.
38. Siegrist, A. E.; Duenenberger, M. E. Swiss Pat. 383985 (1965).
39. Hamciuc, E.; Hamciuc, C.; Cazacu, M. *Eur. Polym. J.* **2007**, *43*, 4739.
40. Franco, O.; Orgzall, I.; Reck, G.; Stockhause, S.; Schulz, B. *J. Phys. Chem. Solids* **2005**, *66*, 994.
41. Liou, G.-S.; Lin, H.-Y.; Hsien, Y.-L.; Yang, Y.-L. *J. Polym. Sci. Part A: Polym. Chem.* **2007**, *45*, 4921; and references therein.
42. Soliman, A. A.; Linert, W. *Thermochim. Acta* **1999**, *338*, 67.
43. Mohamed, G. G.; Omar, M. M.; Hindy, A. H.; Turk, J. *Chem.* **2006**, *30*, 361.
44. Philip, V.; Suni, V.; Prathapachandra Kurup, M. R.; Nethaji, M. *Polyhedron* **2006**, *25*, 1931.
45. Wang, G.; Chang, J. C. *Synth. React. Inorg. Met.-Org. Chem.* **1994**, *24*, 623.
46. Nakamoto, K. Infrared and Raman Spectra of Inorganic and Coordination Compounds; Wiley: New York, **1986**; p 203.
47. Lever, A. B. P.; Mantovani, E. *Can. J. Chem.* **1973**, *51*, 1567.
48. Lever, A. B. P.; Mantovani, E. *Inorg. Chem.* **1971**, *10*, 817.
49. Al-Ghamdi, R. F.; Fahmi, M. M.; Mohamed, N. A. *Polym. Degrad. Stab.* **2006**, *91*, 1530.
50. Kaya, İ.; Koyuncu, S.; Çulhaoğlu, S. *Polymer* **2008**, *49*, 703.
51. Vlad, A.; Zaltariov, M. F.; Shova, S.; Novitchi, G.; Varganici, C. D.; Train, C.; Cazacu, M. *CrystEngComm* **2013**, *15*, 5368.
52. Samal, S.; Das, R. R.; Dey, R. K.; Acharya, S. *J. Appl. Polym. Sci.* **2000**, *77*, 967.
53. Samal, S.; Das, R. R.; Sahoo, D.; Acharya, S.; Panda, R. L.; Rout, R. C. *J. Appl. Polym. Sci.* **1996**, *62*, 1437.
54. Samal, S.; Mohapatra, N. K.; Acharya, S.; Dey, R. K. *React. Funct. Polym.* **1999**, *42*, 37.
55. Wang, L.; Zhu, W.; Fang, M.; Zhang, Q.; Li, C. *Spectrochim. Acta A* **2013**, *109*, 186.
56. Miller, R. D.; Michl, J. *Chem. Rev.* **1989**, *89*, 1359.
57. Yang, C. J.; Jenekhe, S. A. *Macromolecules* **1995**, *28*, 1180.
58. Kao, K. C. Dielectric Phenomena in Solids; Elsevier Academic: San Diego, **2004**; p 75.
59. Mishra, R.; Rao, K. *J. Solid State Ionics* **1998**, *106*, 113.
60. Mishra, R.; Baskaran, N.; Ramakrishnan, P. A.; Rao, K. *J. Solid State Ionics* **1998**, *112*, 261.
61. Schonhals, A.; Kremer, F. In Broadband Dielectric Spectroscopy; Kremer, F., Schonhals, A., Eds.; Springer-Verlag: Berlin, **2003**; p 59.
62. Ramesh, S.; Arof, A. K. *Mater. Sci. Eng. B* **2001**, *85*, 11.
63. Havriliak, S.; Negami, S. *J. Polym. Sci. Polym. Symp.* **1966**, *14*, 99.
64. Mano, J. F.; Pereira, E. *J. Phys. Chem. A* **2004**, *108*, 10824.
65. Georgoussis, G.; Kanapitsas, A.; Pissis, P.; Savelyev, Y. V.; Veselov, V. Y.; Privalko, E. G. *Eur. Polym. J.* **2000**, *36*, 1113.
66. Psarras, G. C. *Compos. A* **2006**, *37*, 1545.
67. Puertotas, J. A.; Carod, E.; Diaz-Calleja, R.; Cerrada, P.; Oriol, L.; Pinol, M.; Serrano, J. L. *Macromolecules* **1997**, *30*, 773.
68. Jonscher, A. K. Universal Relaxation Law; Chelsea Dielectrics: London, **1996**.